Article

pubs.acs.org/Biomac

Thermal and Structural Properties of Silk Biomaterials Plasticized by Glycerol

Joseph E. Brown,[†] Stephen K. Davidowski,[‡] Dian Xu,[‡] Peggy Cebe,[§] David Onofrei,[∥] Gregory P. Holland,[∥] and David L. Kaplan*[,†]

[†]Department of Biomedical Engineering and [§]Department of Physics and Astronomy, Tufts University, Medford, Massachusetts 02155, United States

[‡]School of Molecular Sciences and the Magnetic Resonance Research Center, Arizona State University, Tempe, Arizona 85287-1604, United States

[∥]Department of Chemistry and Biochemistry, San Diego State University, 5500 Campanile Drive, San Diego, California 92182-1030, United States

Supporting Information

ABSTRACT: The molecular interactions of silk materials plasticized using glycerol were studied, as these materials provide options for biodegradable and flexible protein-based systems. Plasticizer interactions with silk were analyzed by thermal, spectroscopic, and solid-state NMR analyses. Spectroscopic analysis implied that glycerol was hydrogen bonded to the peptide matrix, but may be displaced with polar solvents. Solid-state NMR indicated that glycerol induced β-sheet formation in the dried silk materials, but not to the extent of methanol treatment. Fast scanning calorimetry suggested that β-sheet crystal formation in silk-glycerol films appeared to be less organized than in the methanol treated silk films. We propose that glycerol may be simultaneously inducing and interfering with β-sheet formation in silk materials, causing some improper folding that results in less-organized silk II structures even after the glycerol is removed. This difference, along with trace residual glycerol, allows glycerol extracted silk materials to retain more flexibility than methanol processed versions.

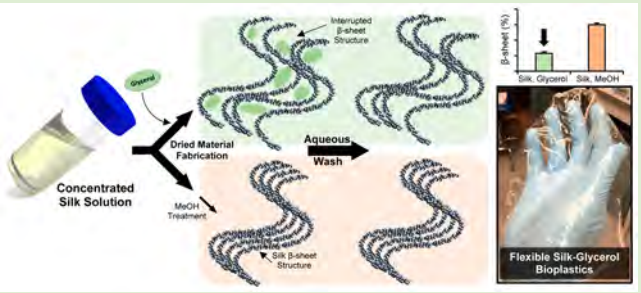

INTRODUCTION

Protein-based thermoplastics are becoming of interest as an alternative to petroleum-based plastics in the food, health and medical industries because of their green origins, biocompatibility, processing versatility, and potentially low cost derivation which does not rely on the market value of crude oil.[1−3] By tuning the mechanical, electrical, and chemical properties of protein bioplastics, several physical characteristics including cellular interactions and in vivo degradation rates can be controlled, a feature that is useful when compared to many synthetic plastics used in the medical industries.[4,5] Regenerated or resolubilized proteins from plant and animal sources (e.g., silk fibroin, wheat gluten, whey protein isolates, zein, among others) often form into dense matrices which generate brittle materials, in contrast to the native proteins.[6] This process ultimately yields materials which may be susceptible to cracking, tearing and plastic deformation, thus less useful for many applications. To overcome the embrittlement of regenerated proteins, plasticizers like polyols, sugars, and lipids have been used.[7−10]

Silk fibroin protein from the *Bombyx mori* caterpillar has become an important candidate for Bioplastic applications due to its mechanical durability, tunable secondary structure, all aqueous processing and purification, and in vivo biocompatibility.[11−13] The silk fibroin heavy chain consists of highly repetitive GAGAGS sequences which participate in protein physical cross-linking and folding.[14] Fibroin peptides can form densely packed, β-pleated sheets when treated with organic solvents like methanol, which leaves the material insoluble in water, but very brittle and rigid when dry. To reduce the rigidity of dried silk materials, the secondary structure and mechanics of silk fibroin materials have been exposed to different hydrophilic, polyol plasticizers, such as glycerol.[15,16] These plasticizers can induce structural changes, resulting in increased crystallinity and β-sheet content, yet the resulting materials are generally softer and highly flexible.

Fourier transform infrared (FT-IR) has previously been used to detect glycerol within silk materials and identify its impact on protein structure.[15,17] Multidimensional solid-state NMR of carbon-13 labeled silk is able to resolve secondary structures such as β-sheets, coil structures, and α-helices for the silk protein,[18,19] while FT-IR can resolve spectral bands correlating

Received: August 22, 2016
Revised: October 31, 2016
Published: November 18, 2016

DOI: 10.1021/acs.biomac.6b01260
Biomacromolecules 2016, 17, 3911−3921

to the presence of glycerol and hydrogen bonding interactions with silk proteins which may impact the stretching vibrations of glycerol. Dynamic mechanical thermal analysis (DMTA) can be used to assess thermal transitions in plasticized systems, such as the glass transition (T_g) and β-relaxations (T_β) in low temperature ranges, while fast scanning calorimetry is key for analyzing high temperature events such as crystal melting which is often obscured in proteins by thermal degradation. Combined, these methods allow insight into glycerol interactions with proteins and whether irreversible physical cross-linking or changes in secondary structure within the protein occur without binding to the glycerol.

The present study was focused on analyzing solid state silk materials with a focus on understanding how glycerol interacts with the silk proteins and in turn, imparts flexibility to the silk materials. Specific interactions between the protein matrices and plasticizers are specific for each system, determined in part based on the polarity, size and shape of the additive, as well as the amino acid sequence and conformation of the protein involved.[6,20,21] Therefore, it is difficult to predict how glycerol affects the folding of silk peptides based on studies with other proteinaceous systems. Glycerol is often considered an external plasticizer, meaning it does not permanently bind to the peptide and is mobile within the protein matrix.[22,23] Therefore, to gain an initial understanding about the role of glycerol on the thermal and structural properties of silk materials, silk films physically cross-linked by methanol or through the incorporation of glycerol were analyzed both before and after extraction of the glycerol from the material.

EXPERIMENTAL SECTION

Materials and Methods. *Preparation of Silk Solutions.* Silk fibroin (hereafter referred to as silk) solution was prepared as previously reported.[24] Briefly, *Bombyx mori* cocoons were boiled in a 0.02 M sodium carbonate solution for 30 min to extract the silk fibroin protein (hereafter referred to as 30 mE, "minutes extracted") and remove the sericin. The extracted silk was washed and dried for 12 h in a chemical hood then dissolved in 9.3 M LiBr solution at 60 °C for 4 h, yielding a 20% w/v solution. This solution was dialyzed for 3 days against distilled water using Pierce Slide-a-Lyzer cassettes, MWCO 3500 Da (Rockford, IL) to remove LiBr. The solution was next centrifuged to remove aggregates that formed during purification. The final solution concentration of silk was ∼6−8% w/v. This concentration was diluted in deionized water to 5% w/v and stored at 2−5 °C until use.

Preparation of ^{13}C Isotopically Labeled Silk. For solid-state NMR studies, silk films were isotopically labeled for determination of silk protein secondary structures. To label silk, a colony of *B. mori* silkworms was raised and fed ubiquitously labeled ^{13}C-glycine and ^{13}C-alanine (Cambridge Isotope Laboratories, Tewksbury, MA, U.S.A.). Enriched food was prepared by adding solubilized amino acid isotopes directly to food (500 mg ^{13}C-glycine and 100 mg ^{13}C-alanine added to 5 g worm food and fed during the fourth and fifth instar stages of the silkworm development). After pupation, the cocoons were collected and stored at 80 °C, and subsequently, the raw cocoons were processed as previously described.

Preparation of Silk-Glycerol Blended Films. Silk protein aqueous solution was mixed with glycerol (Sigma-Aldrich, St. Louis, MO) as described previously.[15] Briefly, glycerol solution at 700 mg/mL was added to silk solutions at various weight:weight (w/w) ratios: 0:100 (silk only controls), 1:99, 5:95, 10:90, 15:85, 20:80, 30:70, and 40:60 weight glycerol/weight silk. Solutions were homogenized via gentle inversion until phase separation was no longer visible. Films were cast from these silk solutions by aliquoting 0.5 mL of solution onto the surface of a 2 cm diameter polydimethylsiloxane (PDMS) discs. Samples were stored inside an air-flow cabinet for 12 h at room temperature until dry. No environmental controls (temperature, humidity) were used during fabrication. In some cases, films were treated in 90% v/v methanol to induce crystallization. For this procedure, films were incubated in methanol for 12 h on a shaker plate at room temperature, then removed from solution and dried in an air-flow hood for an additional 12 h. In the discussion, films tested prior to methanol treatment are referred to as "untreated" or "as cast", while methanol-treated silk only and silk−glycerol films note "MeOH" in the sample title. All films were stored in sealed tubes at room temperature until analysis.

Secondary Structure Analysis of Silk−Glycerol Film by Fourier Transform Infrared (FT-IR). FT-IR and Fourier self-deconvolution (FSD) were used to analyze protein secondary structure for the glycerol-plasticized silk materials. Films were measured using a JASCO FTIR 6200 spectrometer (JASCO, Tokyo, Japan) combined with a MIRacle attenuated total reflection (ATR) germanium crystal. Background and spectral scans were measured from 4000 to 600 cm^{-1} at a resolution of 2 cm^{-1} for 32 scans per sample. Film samples were measured as processed, immediately after drying and postprocessing.

Solution Structure by Circular Dichroism. Silk solutions were diluted 200× (final concentration: 0.01 w/v%) and circular dichroism (CD) spectra were collected using an AVIV Biomedical Model 410 CD spectrometer (Lakewood, NJ), as previously described.[25] Following dilution, solutions were immediately loaded in a 1.0 mm quartz cell (Hellma Analytics, Plainview, NY) within a temperature-controlled cell holder. CD wavelength scans were conducted 3 times at 25 °C between 210 and 260 nm using 0.5 nm steps. Signal intensity data is presented after a seven-point smoothing factor and normalization on a 0 to 1 scale.

Rapid Scan Chip Calorimetry. Fast scanning calorimetry was performed on 10 μm thick silk films as described previously.[26−28] Films were separated into the following groups: (1) silk only, methanol post-treatment; (2) silk with 30% w/w glycerol, no post-treatment; (3) silk with 30% w/w glycerol, methanol post-treatment. Thin film samples were placed on chip sensors and underwent several cycles of thermal scanning in a Flash DSC1 (Mettler Toledo, Zurich, Switzerland). Films were heated at a rate of 2000 K/s to observe the glass transition and endothermic melting peaks. To prevent or minimize degradation, the samples were not heated beyond 380 °C. Several heating cycles were performed to observe irreversible changes in structure after heating to high temperatures.

Solid-State Nuclear Magnetic Resonance (NMR). Solid-state NMR was conducted on silk materials isotopically labeled with ^{13}C-glycine and ^{13}C-alanine. Films were separated into the following groups: (1) silk only, as cast; (2) silk only, methanol post-treatment; (3) silk with 30% w/w glycerol, no post-treatment; (4) silk with 30% w/w glycerol, methanol post-treatment. Solid-state NMR data was collected with a Bruker 400 MHz Avance III spectrometer equipped with a 4 mm CP-MAS probe at 25 °C. Typical experimental parameters for CP-MAS experiments were a 1 ms contact time and 10 kHz MAS with 83 kHz TPPM proton decoupling during acquisition. The ^{13}C direct NMR spectra were collected at 10 kHz MAS with 83 kHz TPPM decoupling and a recycle delay of 10 s (fully relaxed). Data processing, analysis and fitting was done with MestReNova v. 8.0.2. All spectra were zero-filled to 1024 data points and 50 Hz line broadening was applied. The alanine Cβ region of each spectrum was fit with two or three components with fixed chemical shifts at 17.4 ppm (random coil) and 20.2 ppm (β-sheet), respectively. In some cases, a third helical component was required to fit the data. The fitting was repeated 5 times to calculate the mean values of each component and estimate their uncertainties. The two-dimensional (2D) refocused INADEQUATE spectra were collected as previously described[29,30] with 3 ms double quantum (DQ) transfer delays, 10 kHz MAS, and 83 kHz TPPM proton decoupling during the transfers and acquisition.

Thermogravimetric Analysis (TGA). TGA was used to observe interactions between silk, glycerol and adsorbed water. Films were separated into the following groups: (1) silk only, as cast; (2) silk only, methanol post-treatment; (3) silk with 30% w/w glycerol, no post-treatment; and (4) silk with 30% w/w glycerol, methanol post-

DOI: 10.1021/acs.biomac.6b01260
Biomacromolecules 2016, 17, 3911−3921

treatment. Samples were analyzed on Q500 thermogravimetric analysis tool (TA Instruments, New Castle, DE). Samples were preweighed for their initial mass, then were heated at a rate of 10 °C/min from 25 to 800 °C. Mass loss and the derivative mass changes were reported.

Dynamic Mechanical Thermal Analysis (DMTA). The thermoplastic properties of plasticized silk materials were measured using an RSA3 Dynamic Mechanical Analyzer (TA Instruments, New Castle, DE). Films were cut into 10 mm × 5 mm × 0.1 mm dimensions and loaded between stainless steel parallel plates. Liquid nitrogen was used to control the temperature, and mechanical properties were measured during thermal sweeps ranging from −100 to 300 °C. The ramp protocol for each sample consisted of a rapid cooling to −100 °C at a rate of −10 °C/min, a hold for 10 min, then a ramp to 300 °C at a rate of 3 °C/min. The dynamic mechanical features were collected at a strain of 0.1% at 1 Hz, with a max applied strain of 10% and a max allowed force of 250 g. The program was set to auto adjust strain as the sample was heated to maintain contact with the sample and avoid artifacts resulting from film slack. Data was reported as the storage modulus, E', and tan(δ) (the ratio of loss modulus to storage modulus) over a set temperature range.

RESULTS AND DISCUSSION

Secondary Structure Analysis of Plasticized Silk Films by FT-IR. Adsorption bands from 1150 to 800 and 3600−3000 cm^{-1} correlate to interactions between proteins (e.g., soy protein and whey protein isolates) and glycerol.[31−33] Absorption peaks at 850, 925, and 995 cm^{-1} correlated to the C−C stretching peaks in glycerol, and bands at 1045 and 1117 cm^{-1} correlated to C−O for the C_1/C_3 carbons and the C_2 carbon of glycerol, respectively. Silk−glycerol films prior to methanol post-treatment showed peaks in all five of these locations, with absorption intensities correlating to the increased presence of glycerol content (Figure 1, top). All peaks with the exception of the band at 1045 cm^{-1} did not shift position with increased glycerol. The band at approximately 1045 cm^{-1} shifted to a lower energy state as glycerol was added to the system, toward the location of the peak for pure glycerol.

The IR spectra of silk-glycerol films after methanol extraction showed that glycerol peaks from 1150 to 800 cm^{-1} were reduced, indicating that much of the glycerol had been displaced and washed out by the methanol treatment (Figure 1, middle). In the high glycerol concentration groups (i.e., 40% w/w glycerol), there were still peaks present, particularly near 1045 cm^{-1}, suggesting some glycerol remains in the films. In films prior to methanol extraction, the IR spectra for silk only and 1:99 glycerol/silk (w/w) films nearly overlay, suggesting that the lower detection level for glycerol is at approximately 1% w/w in the silk film, which corresponds to approximately 0.25 mg glycerol in a 25 mg film.

Bands in the range of 3600−3000 cm^{-1} represent free and bound −NH and −OH groups and the bands in Figure 1, bottom, were normalized for comparison of line shapes. Band intensity increased as glycerol concentration increased, as expected due to the hydroxyl groups present on glycerol. Band narrowing was observed at high glycerol concentrations and after methanol post-treatment.

The IR spectra for silk films with varying glycerol concentrations suggested interactions with the silk protein. The presence of a shift may indicate that the terminal C−O regions of the glycerol are interacting with the silk, causing a slight change in the stretching vibrations detected by IR. These are prominent in the terminal carbons most likely because these are more accessible in glycerol and elicit the strongest reactions with silk. Band narrowing at the 3300 cm^{-1} peak has been attributed to moisture content and protein cross-linking.[34]

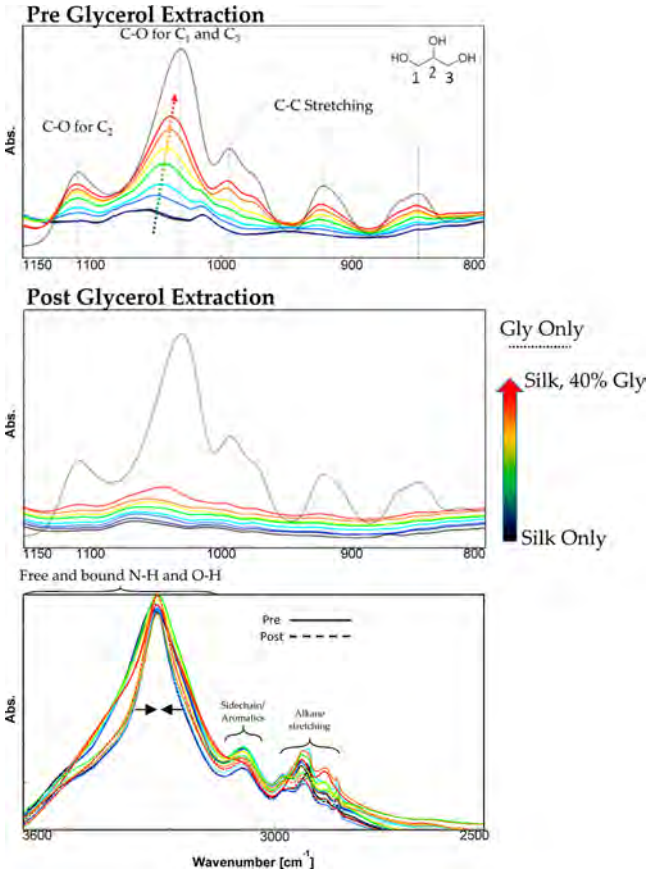

Figure 1. IR spectra for bands representing silk-glycerol films before and after methanol post-treatment. Glycerol concentration in films ranged from 0 to 40% by mass. Top and middle: fingerprint region for glycerol. Five distinct absorbance peaks represent the different stretching vibrations for glycerol. After methanol extraction a majority of the glycerol in the films appears to be removed. Bottom: bands representing free hydroxyl groups in the protein matrix. Solid lines represent films before methanol post-treatment; dotted lines represent films after methanol post-treatment. Band narrowing is indicative of protein crystallization, which occurs at high glycerol concentration and after methanol treatment.

Broader peaks and shoulders in this region may be indicative of the presence of hydroxyl interactions. Protein cross-linking reduces the number of available sites for hydrogen bonding since chains are closer together, thus narrowing this band. At 30 and 40% w/w glycerol (Figure 1, orange and red bands, respectively), the presence of glycerol causes silk to physically cross-link via β-sheet formation.[16] Hence, band narrowing in these spectra is likely attributed to the increase in protein physical cross-linking. This suggests that most of the glycerol has been removed after methanol treatment. Further characterization will be required to determine if glycerol remains at trace amounts or how glycerol content is affected by solvent extraction and duration (i.e., is it possible to remove 100% of glycerol from the silk material). The bands at 3300 cm^{-1} are narrower than premethanol-treated films, likely explained by both methanol induced β-sheet formation in silk and glycerol displacement by extraction.

Secondary Structure of Glycerol-Plasticized Silk Films by Solid-State NMR. Typically, the amide I and II IR regions of silk are used to assess silk secondary structures. Unfortunately, the presence of water may cause artifacts in

DOI: 10.1021/acs.biomac.6b01260
Biomacromolecules 2016, 17, 3911−3921

structure quantification since the absorption peak for water overlaps with the amide I band. Therefore, an alternate, more sensitive approach to uncovering silk secondary structural content was through solid-state NMR analysis of isotopically ^{13}C-labeled silk protein and ^{13}C-labeled glycerol. NMR spectra for films prepared from untreated silk only, silk post-treated in methanol, blended silk−glycerol films, and blended silk−glycerol post-treated in methanol are shown in Figure 2 and Supporting Information, Figure S1. In the top panel, the full spectra for silk films can be seen. For the silk−glycerol films, distinct peaks are observed for glycerol; however, after methanol extraction, these peaks are no longer visible, suggesting removal of the glycerol, as seen in the FT-IR data. The bottom panels depict specific alanine Cβ and carbonyl interactions in the silk protein secondary structure. The methanol post-treatment caused an increase in β-sheet content. Alternatively, blending glycerol into silk films also resulted in an increase in β-sheet content compared to untreated silk, but preserved some of the random coil structure compared to methanol treatment. Finally, extracting silk-glycerol films with methanol further increased the β-sheet content, however, the random coil structure was preserved.

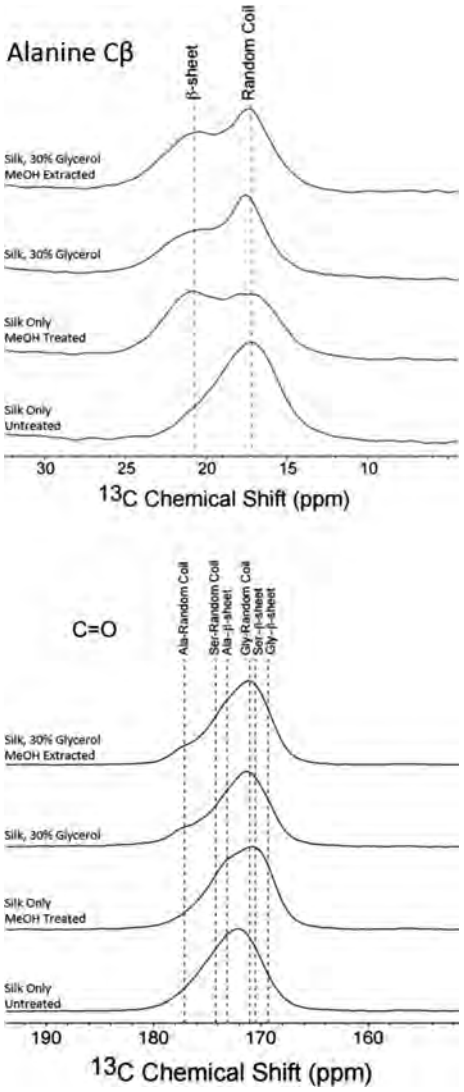

Figure 2. Solid-state NMR spectra for ^{13}C-labeled silk films either as cast ("silk only"), methanol treated, or blended with glycerol. Top: alanine Cβ resonance indicating different secondary structures. Glycerol extraction by methanol caused a large shift in β-sheet content, while glycerol depressed β-sheet formation and increased random coil. Bottom: carbonyl (C═O) resonances from serine, glycine, and alanine in the silk structure.

2D refocused INADEQUATE solid-state NMR experiments were used to extract the conformation dependent chemical shifts for Ala, Gly, and Ser. This experiment allows one to resolve considerably more resonances compared to the 1D ^{13}C experiments (see Figure 3), particularly in the carbonyl region. As can be seen in the figure, distinct carbonyl resonances for β-sheet and random coil structures are observed for the processed films, while the silk film without processing is dominated by random coil shifts. The extracted ^{13}C chemical shifts are presented in Supporting Information, Table 1.[35−38]

The relative contents of β-sheet, coil and coil/helix structures were quantified by peak fitting the alanine Cβ resonances (Figure 4). Methanol treatment increased the β-sheet content in unmodified silk from 37.7 to 64.0% (relative concentration); however, glycerol reduced the β-sheet content to approximately 60%, even with methanol treatment. Random coil content in all samples was reduced compared to untreated "as cast" silk films. Coil structures decreased from 62.3 to 36.0% in methanol-treated silk only films, while glycerol resulted in approximately 40.0% coil structure, regardless of methanol treatment. These results suggest that glycerol may disrupt some of the formation of β-sheet structure, and β-sheet content was not recovered fully even after methanol treatment, at least compared to silk only films after methanol treatment. Alternatively, glycerol preserves more of the disordered coil structures. Thermal measurements from the fast scanning calorimetry confirm that this disruption of β-sheet crystal formation alters the physical properties of silk materials and appears to be a permanent change even after removal of the majority of glycerol by methanol.

Dynamic Mechanical Thermal Analysis (DMTA). DMTA was used to characterize silk materials plasticized by glycerol. The solid lines represent the storage modulus, E', a measure of the elastic behavior of the protein, while the dotted lines represent tan(δ) which defines the overall viscoelastic properties of the materials by providing a ratio of the loss modulus (E'') to the storage modulus. Increases in the viscous component, or decreases in the elastic component both elicit an increase in tan(δ) peak and intensity, which generally occurs during thermal transitions. Silk films as cast (no post-treatment) were predominantly amorphous in structure, with limited β-sheet formation (Supporting Information, Figure S2). The glass transition of these materials was approximately 190 °C, represented by a sharp tan(δ) peak and rapid decrease in modulus as the material transitioned from a brittle glass to soft rubber. The presence of β-sheet structure resists thermal relaxation to a rubbery state, hence, methanol-treated silk films exhibited a shift in glass transition to a higher temperature, approximately 220 °C. Additionally, a crystallization peak was observed at high temperatures for amorphous, as cast films, only when high temperatures induced a spontaneous reorganization of protein amorphous structures to crystalline structures. This was evidenced by the increase in material stiffness between 210 and 250 °C. In silk films treated with methanol, most of the protein available for physical cross-linking has already undergone conversion to crystalline form; hence, a crystallization peak was not observed in these materials. At very high temperatures (>250 °C), the silk

DOI: 10.1021/acs.biomac.6b01260
Biomacromolecules 2016, 17, 3911−3921

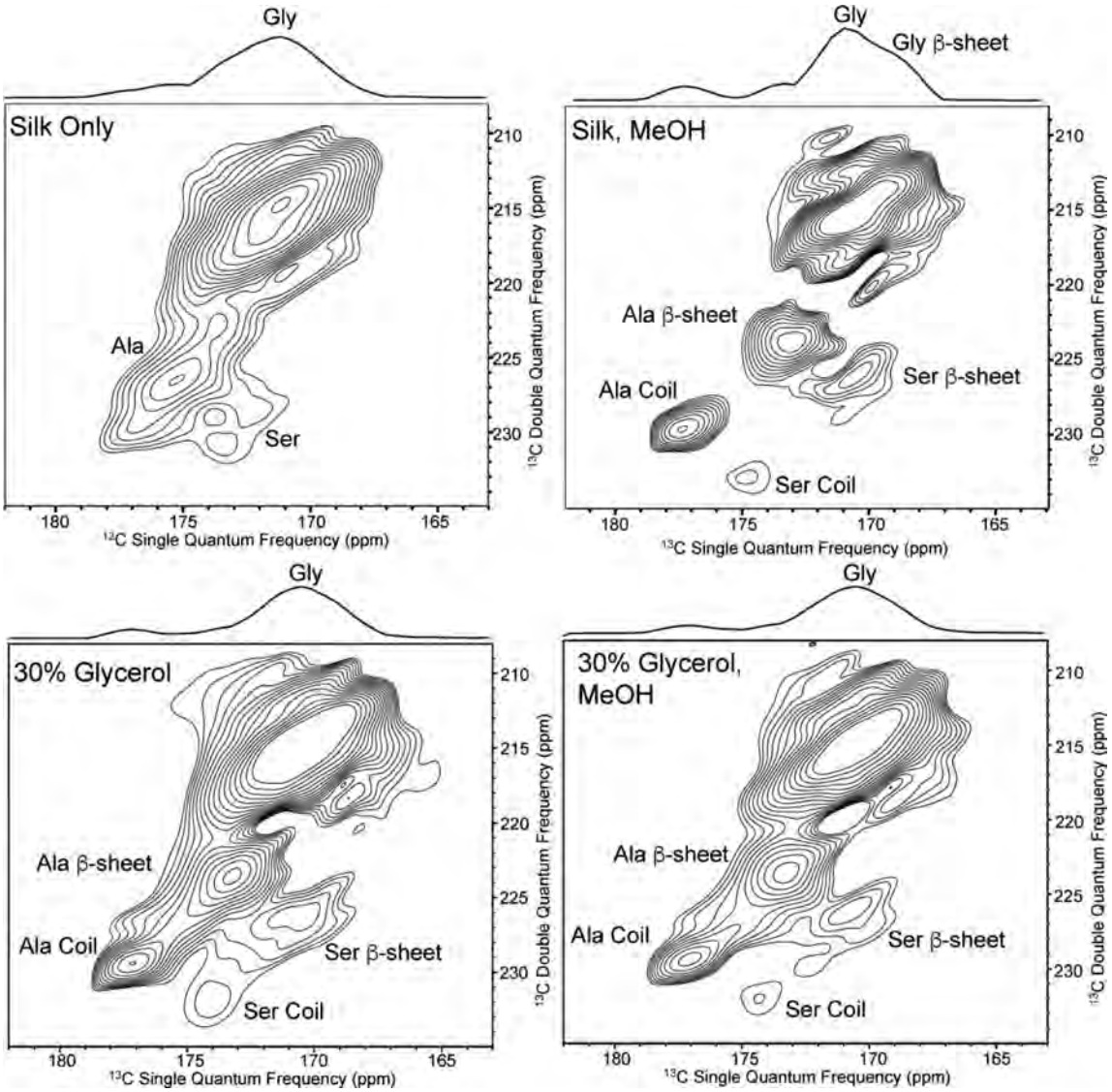

Figure 3. 2D Refocused INADEQUATE solid-state NMR spectra for ^{13}C-labeled silk films either as cast ("silk only"), methanol treated, or blended with glycerol. Carbonyl resonances indicating different secondary structures for alanine and serine in processed silk films are indicated. Glycerol extraction by methanol caused a large shift in β-sheet content, while glycerol depressed β-sheet formation and increased random coil.

materials begin to degrade, a sharp decline in storage modulus was observed, and the films were no longer fully intact.

The thermoplastic behavior of silk−glycerol films was measured at varying weight concentrations of glycerol (Figure 5 and Supporting Information, Figure S3). A defining feature of plasticization in polymeric materials is both reduction of material stiffness and depression of the glass transition temperature in a concentration-dependent manner. In Figure 5, silk films exhibited softening and a reduction in the storage modulus as glycerol content is increased. At low concentrations of glycerol (i.e., 5% w/w), a sharp reduction in storage modulus at the T_g was observed, as well as an increase in E' after the glass transition, suggesting heat-induced crystallization. At 15% glycerol, the glass transition temperature peak was broader, and the storage modulus was slightly reduced at ambient temperature. Compared to the methanol-treated silk films, both 5 and 15% glycerol plasticized the silk by depressing T_g. No obvious T_c was detected for 15% glycerol, indicating that β-sheet may spontaneously form in these materials. At 30% glycerol, a very different profile was observed compared to the other films. The storage modulus steadily declined as the temperature increased, with only a small plateau around 0−50 °C. Additionally, tan(δ) peaks for T_g were very broad and spanned from 0 to 200 °C.

DMTA was also used to observe the effects of post-treatment extraction steps on silk-glycerol films in either methanol or deionized water. As mentioned previously, the expectation is that polar solvents displace glycerol from the silk materials. Instead of directly measuring the residual glycerol content in silk materials, DMTA can be used to indirectly measure the effects of extraction, to assess residual physical effects postextraction. Extraction of silk-glycerol films for 12 h in methanol reduced the plasticization effect of glycerol in these films (Figure 6, Supporting Information, Figure S4). After extraction, the T_g was approximately the same as for the silk MeOH-treated films, suggesting that most of the glycerol was removed and the thermoplastic properties resemble those of a nonplasticized material. However, it was possible to recapitulate the plasticization of silk films by extracting them in glycerol (Figure 6, bottom). Films immersed into a glycerol solution (90:10 v/v glycerol/water) after methanol extraction had

DOI: 10.1021/acs.biomac.6b01260
Biomacromolecules 2016, 17, 3911−3921

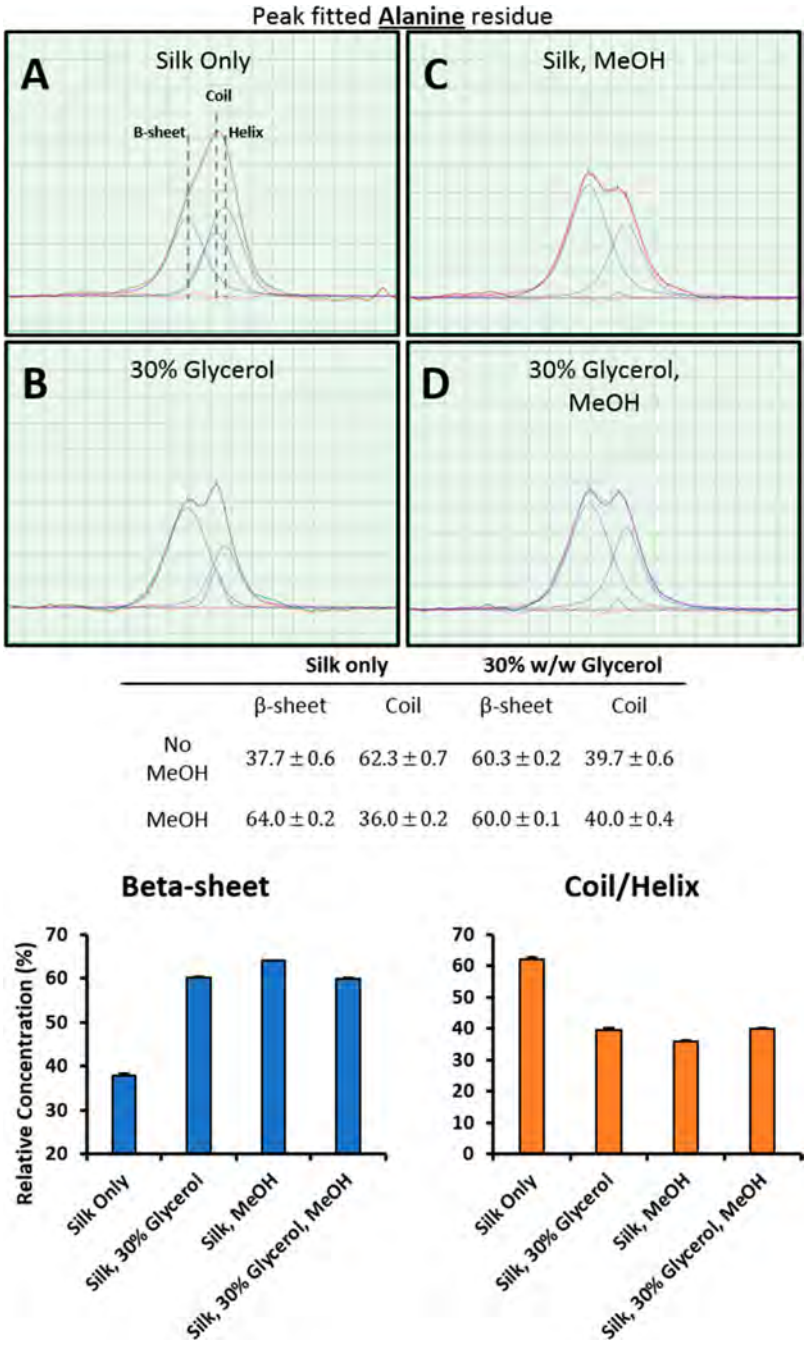

Figure 4. Quantitative analysis of solid state NMR spectra for silk materials. Curve fitting results for NMR data were reported at the average ± standard deviation for $N = 5$.

mechanical properties and a T_g peak profile similar to the original silk−glycerol films.

Dynamic mechanical thermal analysis measures the viscoelastic behavior of films across a broad temperature range in order to observe thermal transitions of the material. This method is useful for detecting subtle protein relaxations such as local β-relaxations, as well as more global relaxations such glass transitions. Thermal transitions were detected in silk films either with or without methanol post-treatment (Supporting Information, Figure S2). A few noticeable peaks included the β-relaxations (T_β), which are primarily attributed to protein−water interactions,[39] glass transition or α-relaxation (T_α), which is associated with a physical transition from a brittle, glassy state to a soft, rubbery state, and crystallization temperature (T_c), which is the temperature where amorphous protein structures spontaneously reassemble into crystalline structures.[40,41] These transitions, particularly the glass transition, define the thermoplastic behavior of a particular material, which may be useful in determining functionality in several applications. Thus, the reduction of the glass transition temperature and material stiffness via the addition of glycerol could be used to design soft, flexible silk materials that could undergo thermal transitions at lower temperatures for processing applications such as thermal molding or fused deposition in 3D printing, or to further study drug stability properties in silk matrices.[42,43]

Thermogravimetric Analysis (TGA). Thermogravimetric analysis was performed to observe the behavior of silk materials blended with plasticizer and after solvent washing treatment.

DOI: 10.1021/acs.biomac.6b01260
Biomacromolecules 2016, 17, 3911−3921

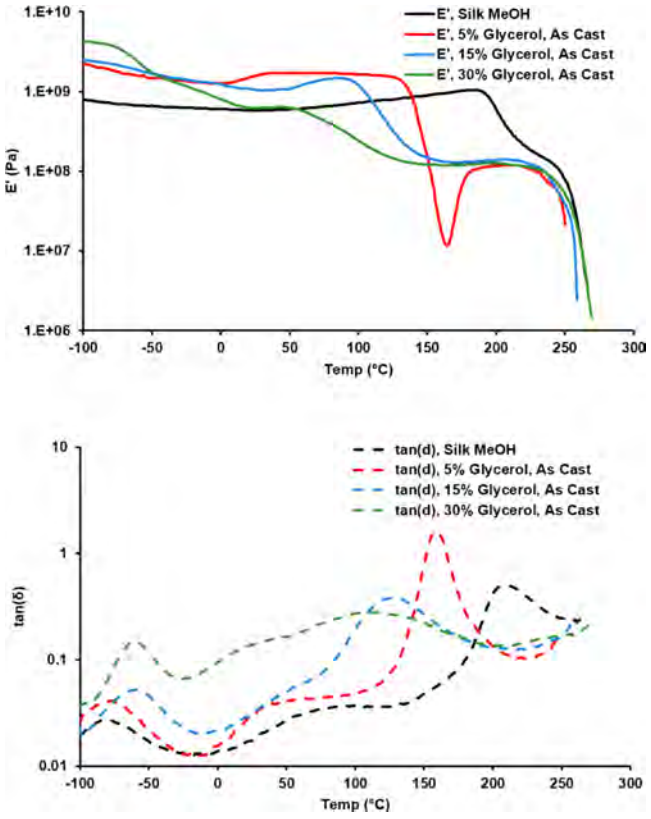

Figure 5. DMTA of silk−glycerol films at varying weight fractions of glycerol. As glycerol was increased, two trends were observed. First a decrease in the storage modulus over the temperature range tested indicated that glycerol addition softened the silk films. Second, the glass transition peak shifted to a lower temperature as glycerol increased, a common characteristic of plasticization.

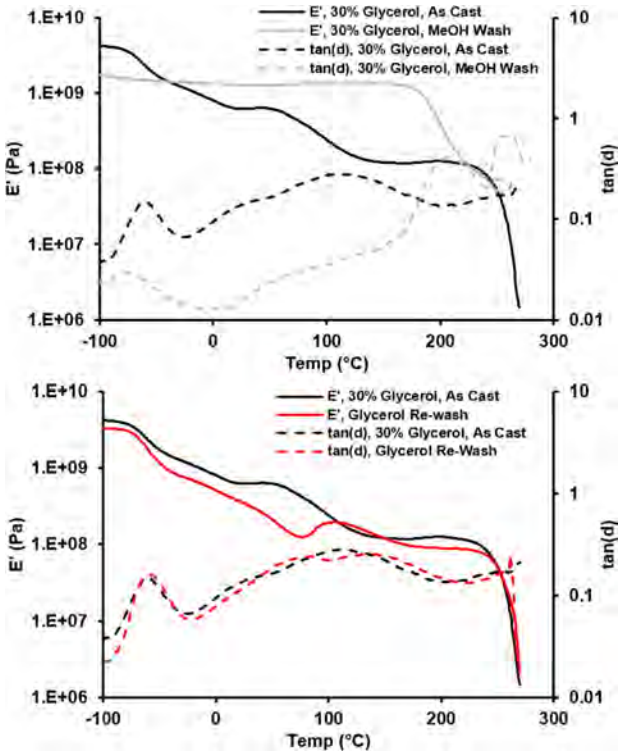

Figure 6. DMTA of silk-glycerol films with various post-treatment extraction steps. Top: Silk−glycerol films extracted in methanol, resulting in the reduction of plasticization effects of glycerol after it was displaced by solvent. Bottom: After films were extracted in methanol to remove glycerol, immersion in a glycerol solution resulted in recapitulation of plasticization.

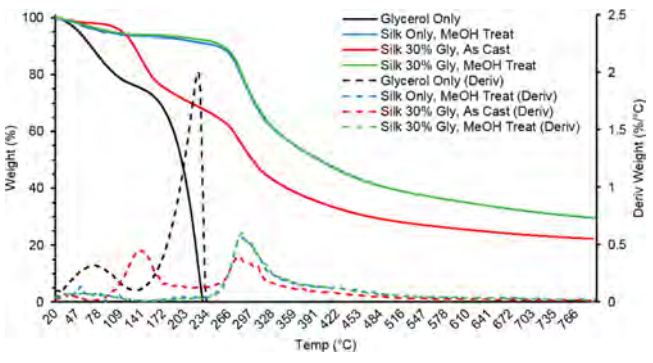

Figure 7. Thermogravimetric analysis of glycerol-plasticized silk films. Solid lines denote weight loss profiles, while dotted lines signify weight loss derivatives.

Figure 7 compares silk−MeOH-treated films with silk−glycerol (30% w/w) films and glycerol only solution. Glycerol alone shows two derivative peaks: one likely attributed to water evaporation (up to approximately 100 °C) and one attributed to evaporation of glycerol (at approximately 222 °C). Silk−MeOH films show gradual water evaporation up to approximately 110 °C, as well as a thermal degradation peak at 287 °C, similar to the degradation temperature found by DMTA. In silk−glycerol films, three phases are detected, likely due to the evaporation of water, then glycerol, and then silk degradation. In glycerol, a derivative peak at 72 °C was attributed to water evaporation; however, in silk−glycerol films, this peak appears to shift to 142 °C. This may be due to enhanced stability of water within the silk−glycerol matrix. In the region from approximately 160−270 °C, a gradual decrease in mass is observed as temperature is increased. It is hypothesized that due to a variety of interactions glycerol may have within the silk matrix (e.g., glycerol−peptide interactions), a range of glycerol volatilities are observed, resulting in gradual evaporation opposed to a sharp decline. The less stable interactions allow glycerol evaporation at lower temperatures, while the more stable interactions are removed closer to 270 °C. Methanol-extracted silk−glycerol films appear similar to those of silk−MeOH films, suggesting that glycerol has been removed from the sample.

Fast Scanning Calorimetry (FSC). Figure 8 shows heating scans for silk films either post-treated in methanol, blended with 30% w/w glycerol, or having both blended glycerol modification and methanol treatment. Red curves indicate the initial heating scan at 2000 K/s, while blue curves represent the second thermal cycle (after cooling at 2000 K/s). The second scan is used to verify the amorphous nature of the samples after crystal melting in the first heating scan. In silk−MeOH crystalline samples, a T_g at approximately 240 °C was detected. In the reheating scan, the now-amorphous sample has its T_g lowered to about 210 °C, consistent with our previous report on amorphous silk.[29] Compared to the DMTA data, thermal transitions like that at T_g will be shifted to higher temperatures in fast scanning calorimetry due to the greatly increased rate of heating. However, trends in glass transition relative to each group agree between the two analytical methods, confirming the results observed with DMTA.

DOI: 10.1021/acs.biomac.6b01260
Biomacromolecules 2016, 17, 3911−3921

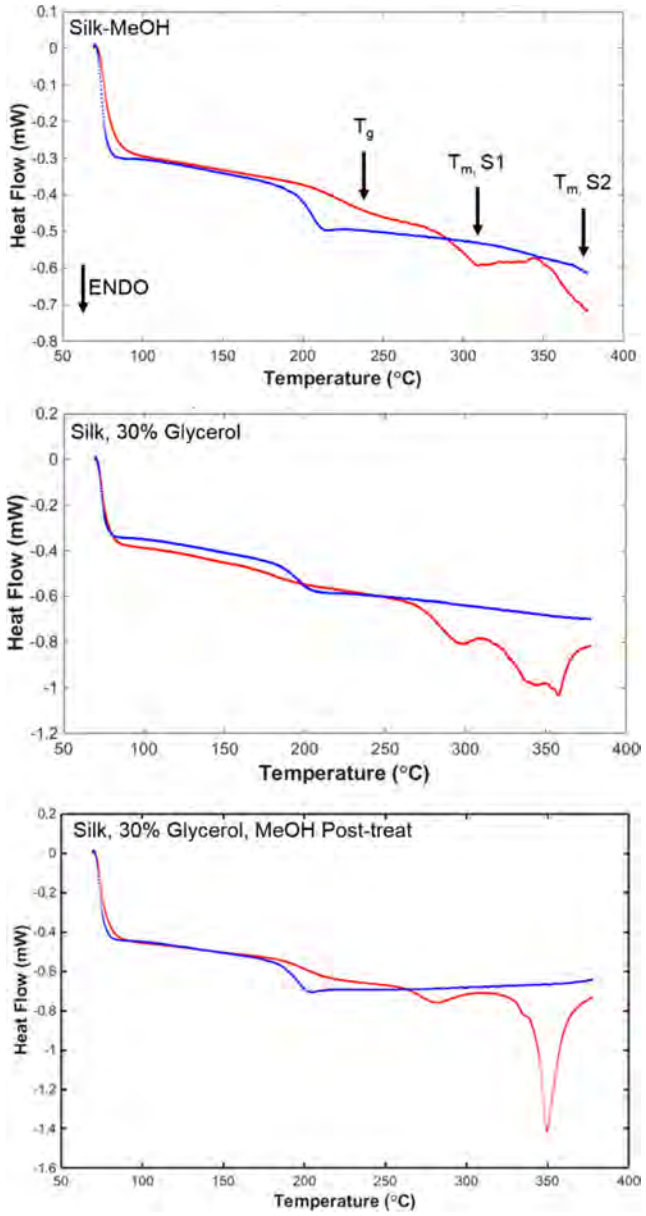

Figure 8. Fast scanning calorimetry at 2000 K/s of silk films: red curves represent first heating scan, blue curves represent the second thermal scan after crystal melting has occurred. Top panel: silk–MeOH-treated films exhibited a glass transition at ~240 °C, with one complete and one incomplete melting endotherm, likely representative of silk I and silk II crystal structures, respectively. Middle panel: silk with 30% w/w glycerol exhibited a depressed T_g compared to silk–MeOH, however, yields two complete melting endotherms. Bottom panel: silk–glycerol films with methanol post-treatment. Two complete melting endotherms were observed. The second melting endotherm was shifted to a lower temperature compared to silk–MeOH, suggesting imperfect formation of silk II crystals.

Two crystal melting endotherms were detected in silk–MeOH films: a complete lower melting endotherm with peak at approximately 300 °C, and an incomplete higher melting endotherm, with peak occurring beyond 370 °C. In DMTA, protein degradation occurred at approximately 280 °C, so these melting transitions observable in FSC, were not detectable using DMTA. In crystalline silk with 30% w/w glycerol, an expected depression of glass transition was observed, and two melting endotherms at 300 and 350 °C were apparent. Finally, silk–glycerol crystalline films with methanol post-treatment exhibited a T_g at approximately 220 °C, between both silk–MeOH and silk–glycerol films. Additionally, two complete melting endotherms were also observed at approximately 280 and 350 °C.

Unlike the DMTA assessments, fast scanning calorimetry is useful for detecting melting temperature transitions which would normally be obscured by protein degradation at slower rates of heating.[26] By heating up to 2000 K/s, we were able to observe crystal melt endotherms in glycerol plasticized silk films. Furthermore, films underwent multiple heating cycles which were able to detect reversible melting of protein crystalline structure and conversion to an amorphous state. As expected, glass transition temperatures were depressed by the addition of plasticizer compared to silk only films crystallized with methanol. As seen in DMTA, the T_g for silk–glycerol was broad, while the transitions for methanol-treated films were sharper. For all samples in FSC, the second thermal sweep showed a sharp glass transition at approximately 200–210 °C. This was due to the complete melting of the crystalline structure during the first thermal cycle. Silk films, regardless of treatment, were all reduced to a completely amorphous structure.

The reason for two high temperature melting endotherms may be due to differences in crystallinity between the materials. For example, this could be due to the presence of large and small crystal aggregates or possibly differences in silk crystal type (i.e., silk I vs silk II structure). This result may also be due to reorganization of some material into a more stable crystalline form during heating. The melting endotherms in silk–glycerol materials were complete, while only one endotherm in the silk–MeOH group was complete. Glycerol appeared to shift the second melting endotherm to a lower temperature. The first endotherm was likely representative of a less stable crystalline silk I structure,[44] while the second endotherm represents a more thermally stable crystal type (silk II, which is described as a hydrogen-bonded, antiparallel β-pleated sheet structure[45,46]). More organized, perfect forming crystals will exhibit a higher melting endotherm and more narrow peak. Silk-MeOH treated films, exhibited the highest β-sheet content conferring a high degree of order and thermal stability. Alternatively, hydrophilic polyol plasticizers like glycerol are believed to form hydrogen bonds between peptide chains,[47] interfering with the formation of peptide linkages. As seen in the NMR data, glycerol induced a conformational shift in silk materials toward a β-sheet structure, but also prevented the formation of the β-sheets to the extent seen with the silk–MeOH samples. This outcome remains even after silk–glycerol materials were post-treated with methanol. If silk II crystals are formed in silk–glycerol materials, they may not be as stable compared to silk II crystals formed from silk–MeOH materials. Therefore, we would expect to observe a depressed melting endotherm for the silk II crystal melting temperature.

Mechanism of Silk–Glycerol Interactions. Previous work has shown that high glycerol concentration induced a conformational change in silk materials from an amorphous structural state to an ordered crystalline state.[15,16] As more glycerol is added to silk films, the transition from glassy to rubbery states was obscured, and no sharp transition was found. The reason for this broad transition may have to do with the silk protein structure. The processing methods used to purify silk protein (boiling and extraction from the cocoon) ultimately yields a polydisperse molecular weight profile of silk proteins

DOI: 10.1021/acs.biomac.6b01260
Biomacromolecules 2016, 17, 3911–3921

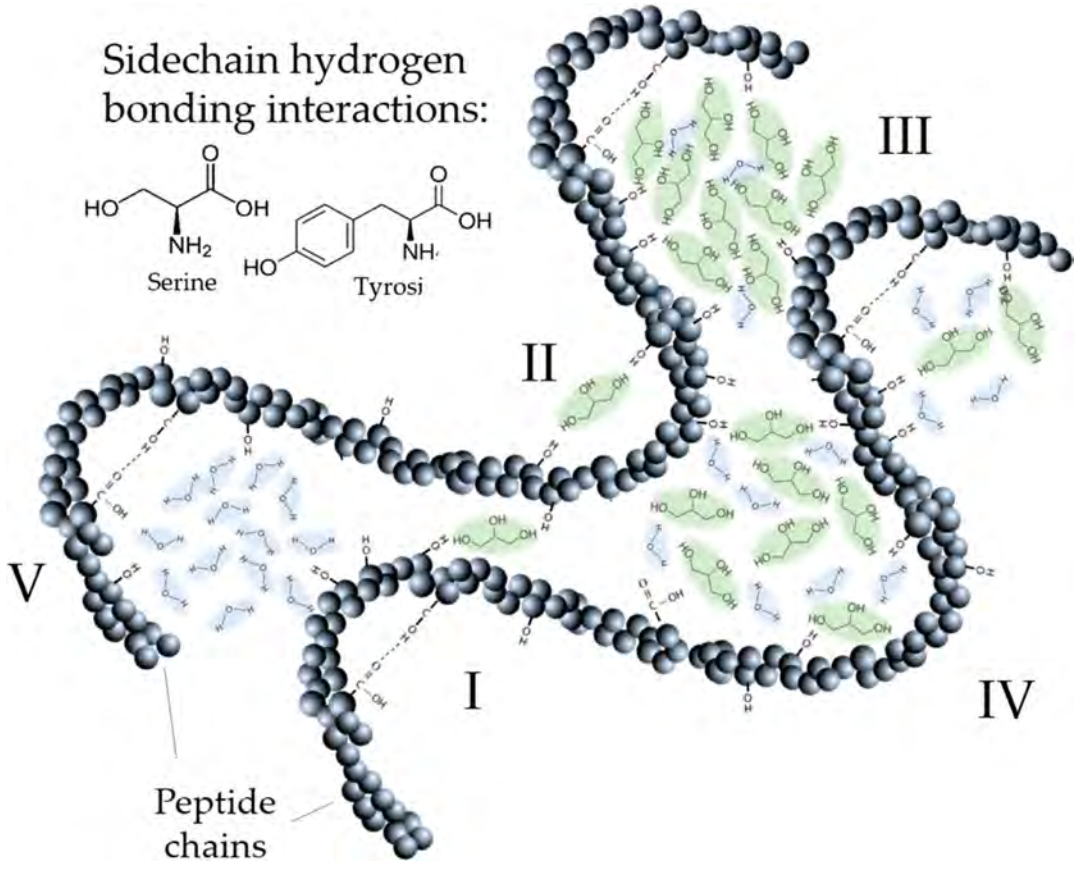

Figure 9. Proposed mechanism of plasticizer effect on silk films. There are likely at least five distinct types of peptide interactions occurring in plasticized systems. Numbered regions as follows: (I) peptide−peptide hydrogen bonding and physical cross-linking, as seen in β-sheet formation; (II) glycerol bridges, where one glycerol molecule is linked to two separate peptide chains; (III) local glycerol-rich domain, where glycerol molecules are interacting with both the peptide chains as well as other glycerol molecules; (IV) glycerol−water domains, similar to part III, except hydrogen bonding occurs with water molecules as well; (V) due to disruption of hydrogen bonding during silk protein conformational shift toward β-sheet formation, hydrogen bonding sites are subsequently available for interaction by water molecules in aqueous media. This would explain enhanced water uptake in silk−glycerol modified materials, even after removal of glycerol. It is hypothesized that glycerol interactions occur predominantly with serine and tyrosine residues due to their polar side chains.

ranging from 40 to 350 kDa.[48] The different molecular weight protein fragments may interact differently (via either peptide−peptide or peptide−glycerol interactions) within the mixture, yielding a broad glass transition temperature. An alternative explanation may have to do with the variations in secondary structure as higher concentrations of glycerol are blended into the protein solution. Peptide cross-linking and stable β-sheet structures typically resist thermal transitions in polymeric systems, therefore, eliciting higher glass transition temperatures; however, as glycerol may cause imperfections by preventing the formation of tightly physically cross-linking peptide crystals, we may be observing a broad population of structures with different degrees of imperfection. Regions of silk matrices with higher interference from glycerol interactions may relax as lower temperatures than more ordered regions, hence the disappearance of a strong peak.

A proposed schematic of the mechanisms of interaction between the silk and glycerol is shown in Figure 9. There are likely five (if not more) types of peptide interactions occurring within the plasticizer interactions: (I) Peptide−peptide linkages and hydrogen bonding witnessed in typical β-sheet cross-linking. (II) Glycerol bridges exhibiting hydrogen bonding interactions with two peptide chains on each glycerol molecule. (III) Local glycerol-rich domain, which occurs when large concentrations of glycerol are added to a protein matrix, likely resulting in hydrogen bonding to silk peptides as well as other glycerol molecules. This can cause a phase separation by glycerol rich areas between peptide chains. (IV) Occurring during immersion of the glycerol-plasticized silk material into aqueous media. Hydrogen bonding interactions may occur more frequently between glycerol and water molecules. These interactions may assist in the extraction of glycerol from the silk matrix. (V) Due to the disruption of peptide−peptide physical cross-linking and hydrogen bonding, protein folding results in the stable formation of an insoluble protein material with reduced β-sheet structure as evidenced from the FTIR and NMR data. This type of physical cross-linking leaves exposed reactive sites available for water or other small polar molecules to interact via hydrogen bonding. The residues most likely participating in glycerol interactions are either tyrosine or serine, due to their hydrophilic side chains. Most likely serine contributes more than tyrosine due to the steric hindrance of the phenolic ring structure in tyrosine as well as the higher mole percent of serine in the chains. The near perfect overlay of original silk−glycerol and glycerol re-extraction data indicates that glycerol is able to interact with silk protein matrices in a similar extent as with the original material. This may not be possible if active sites on the peptide chain are involved in

DOI: 10.1021/acs.biomac.6b01260
Biomacromolecules 2016, 17, 3911−3921

stable peptide−peptide interactions, suggesting that glycerol disruption may cause permanent defects in the silk crystalline structure, resulting in retention of the more flexible material features.

In silk materials, two processes are simultaneously occurring with glycerol plasticization: an increase in chain mobility that leads to spontaneous rearrangement into β-sheet structure, as well as physical cross-link (β-sheet) interruption by glycerol. The result is an insoluble, cross-linked material which has a reduced physical cross-link content compared to silk materials treated with nonglycerol methods (e.g., methanol). In methanol post-treatment, there is no interference (or limited interference) in β-sheet formation, and the stable product is a brittle, highly cross-linked material. Glycerol, however, disrupts this cross-linking, and after extracting the glycerol by solvent post-treatment, the protein does not revert back to a fully physically cross-linked format. Therefore, active and available hydration sites, which would have normally been involved in peptide−peptide interactions, are now reactive with water molecules, or other polar solvents. This finding has significant implications for the formation of less brittle silk materials.

CONCLUSIONS

The ability to induce crystallinity and insolubility in silk materials without the addition of solvents like methanol is a useful alternative as it allows fabrication of soft, flexible, and biocompatible materials capable of interfacing with cells and other biological molecules. The thermoplastic behavior of these silk-glycerol films is useful because it indicates that silk material softening (by glass transition and glycerol-induced flexibility) could be useful for certain processing applications, such as filament printing or thermal molding. Typically for protein systems, the glass transition temperature indicates a state where materials are flexible and ductile, allowing processing and manipulation that would not be possible at lower temperatures when protein-based materials are brittle. Though a glass transition temperature exists for nonplasticized proteins, this transition temperature often overlaps with the degradation temperature, causing materials to char, denature or burn. Plasticizer addition widens the gap between glass transition and degradation temperatures, creating a workable temperature range where proteins can exist a rubber transition without degradation. This opens the door for certain processing applications such as filament printing or thermal molding that would otherwise not be possible with protein-based materials such as silk.

The work presented here provides a basis for predicting the physical outcomes of silk biomaterials plasticized by glycerol. The need still exists to understand how and to what extent residual glycerol plays a role in the physical properties of the silk materials. Initial data suggests that almost all of the glycerol in the silk blended materials is extracted when incubated in either water or methanol, yet these materials are still more flexible than their silk only counterparts, suggesting some residual glycerol in the materials may also be important. Understanding these types of interactions will assist in designing novel, complex materials for biomaterials for a range of utilities, from medical devices and implants to cell substrates and injectable materials. Applying the understanding developed in this work for glycerol interference in silk secondary structure formation may also be relevant to other protein systems where protein secondary structure and folding are critical for the final material properties.

ASSOCIATED CONTENT

Supporting Information

The Supporting Information is available free of charge on the ACS Publications website at DOI: 10.1021/acs.biomac.6b01260.

Expanded solid-state NMR spectra for Figure 2, as well as background DMTA data supplementing Figures 5 and 6 (PDF).

AUTHOR INFORMATION

Corresponding Author

*E-mail: david.kaplan@tufts.edu. Tel.: +1-617-627-3251. Fax: +1-617-627-3231.

ORCID

David L. Kaplan: 0000-0002-9245-7774

Notes

The authors declare no competing financial interest.

ACKNOWLEDGMENTS

P.C. acknowledges Prof. Christoph Schick for providing access to the Mettler Flash DSC1 at the Institute for Physics, University of Rostock, Rostock, Germany. P.C. thanks NSF and DAAD for support during her stay at the University of Rostock, Rostock, Germany. G.P.H. acknowledges DOD-AFOSR and D.L.K. acknowledges AFOSR (FA9550-14-1-0015) and DTRA for support.

REFERENCES

(1) McKeen, L. W.*Plastics Used in Medical Devices*; Elsevier Inc., 2014.
(2) Shah, A. A.; Hasan, F.; Hameed, A.; Ahmed, S. *Biotechnol. Adv.* **2008**, *26* (3), 246−265.
(3) Siracusa, V.; Rocculi, P.; Romani, S.; Rosa, M. D. *Trends Food Sci. Technol.* **2008**, *19* (12), 634−643.
(4) Hu, X.; Cebe, P.; Weiss, A. S.; Omenetto, F.; Kaplan, D. L. *Mater. Today* **2012**, *15* (5), 208−215.
(5) Irimia-Vladu, M.; Głowacki, E. D.; Voss, G.; Bauer, S.; Sariciftci, N. S. *Mater. Today* **2012**, *15* (7−8), 340−346.
(6) Athamneh, A. I.; Griffin, M.; Whaley, M.; Barone, J. R. *Biomacromolecules* **2008**, *9*, 3181−3187.
(7) Cherian, G.; Gennadios, A.; Weller, C.; Chinachoti, P. *Cereal Chem.* **1995**, *72*, 1−6.
(8) Vieira, M. G. A.; Da Silva, M. A.; Dos Santos, L. O.; Beppu, M. M. *Eur. Polym. J.* **2011**, *47* (3), 254−263.
(9) Bocqué, M.; Voirin, C.; Lapinte, V.; Caillol, S.; Robin, J.-J. *J. Polym. Sci., Part A: Polym. Chem.* **2016**, *54* (1), 11−33.
(10) Pereda, M.; Marcovich, N. E.; Mosiewicki, M. a. *Food Hydrocolloids* **2015**, *44*, 407−415.
(11) Vepari, C.; Kaplan, D. L. *Prog. Polym. Sci.* **2007**, *32* (8−9), 991−1007.
(12) Thurber, A. E.; Omenetto, F. G.; Kaplan, D. L. *Biomaterials* **2015**, *71*, 145−157.
(13) Omenetto, F. G.; Kaplan, D. L. *Science (Washington, DC, U. S.)* **2010**, *329* (5991), 528−531.
(14) Zhou, C. Z.; Confalonieri, F.; Jacquet, M.; Perasso, R.; Li, Z. G.; Janin, J. *Proteins: Struct., Funct., Genet.* **2001**, *44* (2), 119−122.
(15) Lu, S.; Wang, X.; Lu, Q.; Zhang, X.; Kluge, J.; Uppal, N.; Omenetto, F.; Kaplan, D. L. *Biomacromolecules* **2010**, *11* (1), 143−150.
(16) Jose, R. R.; Brown, J. E.; Polido, K. E.; Omenetto, F. G.; Kaplan, D. L. *ACS Biomater. Sci. Eng.* **2015**, *1* (9), 780−788.
(17) Pei, Y.; Liu, X.; Liu, S.; Lu, Q.; Liu, J.; Kaplan, D. L.; Zhu, H. *Acta Biomater.* **2015**, *13*, 168−176.
(18) Asakura, T.; Suzuki, Y.; Nakazawa, Y.; Holland, G. P.; Yarger, J. L. *Soft Matter* **2013**, *9*, 11440.

DOI: 10.1021/acs.biomac.6b01260
Biomacromolecules 2016, 17, 3911−3921

(19) Asakura, T.; Suzuki, Y.; Nakazawa, Y.; Yazawa, K.; Holland, G. P.; Yarger, J. L. *Prog. Nucl. Magn. Reson. Spectrosc.* **2013**, *69*, 23−68.
(20) Sothornvit, R.; Krochta, J. M. *J. Food Eng.* **2001**, *50* (3), 149−155.
(21) Martelli, S. M.; Laurindo, J. B. *Int. J. Polym. Mater.* **2012**, *61* (1), 17−29.
(22) Budhavaram, N. K.; Miller, J. a.; Shen, Y.; Barone, J. R. *J. Agric. Food Chem.* **2010**, *58* (17), 9549−9555.
(23) Rahman, M.; Brazel, C. S. *Prog. Polym. Sci.* **2004**, *29* (12), 1223−1248.
(24) Rockwood, D. N.; Preda, R. C.; Yücel, T.; Wang, X.; Lovett, M. L.; Kaplan, D. L. *Nat. Protoc.* **2011**, *6* (10), 1612−1631.
(25) Yucel, T.; Cebe, P.; Kaplan, D. L. *Biophys. J.* **2009**, *97* (7), 2044−2050.
(26) Cebe, P.; Hu, X.; Kaplan, D. L.; Zhuravlev, E.; Wurm, A.; Arbeiter, D.; Schick, C. *Sci. Rep.* **2013**, *3*, 1130.
(27) Cebe, P.; Partlow, B. P.; Kaplan, D. L.; Wurm, A.; Zhuravlev, E.; Schick, C. *Thermochim. Acta* **2015**, *615*, 8−14.
(28) Hu, X.; Kaplan, D.; Cebe, P. *Macromolecules* **2006**, *39* (18), 6161−6170.
(29) Lesage, A.; Bardet, M.; Emsley, L. *J. Am. Chem. Soc.* **1999**, *121* (22), 10987−10993.
(30) Holland, G. P.; Jenkins, J. E.; Creager, M. S.; Lewis, R. V.; Yarger, J. L. *Chem. Commun.* **2008**, *43*, 5568−5570.
(31) Le Tien, C.; Letendre, M.; Ispas-Szabo, P.; Mateescu, M.; Delmas-Patterson, G.; Yu, H. L.; Lacroix, M. *J. Agric. Food Chem.* **2000**, *48* (11), 5566−5575.
(32) Guerrero, P.; de la Caba, K. *J. Food Eng.* **2010**, *100*, 261−269.
(33) Bergo, P.; Sobral, P. J. A. *Food Hydrocolloids* **2007**, *21*, 1285−1289.
(34) Mateescu, M. A.; Schell, H. D.; Dimonie, M.; Todireanu, S.; Maior, O. *Polym. Bull.* **1984**, *11*, 421−427.
(35) Saitô, H.; Tabeta, R.; Asakura, T.; Iwanaga, Y.; Shoji, A.; Ozaki, T.; Ando, I. *Macromolecules* **1984**, *17* (7), 1405−1412.
(36) Wishart, D. S.; Bigam, C. G.; Holm, A.; Hodges, R. S.; Sykes, B. D. *J. Biomol. NMR* **1995**, *5*, 67−81.
(37) Saito, H. *Magn. Reson. Chem.* **1986**, *24* (10), 835−852.
(38) Saitô, H.; Iwanaga, Y.; Tabeta, R.; Narita, M.; Asakura, T. *Chem. Lett.* **1983**, *12*, 427−430.
(39) Bier, J. M.; Verbeek, C. J. R.; Lay, M. C. *Macromol. Mater. Eng.* **2014**, *299*, 524−539.
(40) Bier, J. M.; Verbeek, C. J. R.; Lay, M. C. *Macromol. Mater. Eng.* **2014**, *299* (1), 85−95.
(41) Guan, J.; Porter, D.; Vollrath, F. *Biomacromolecules* **2013**, *14* (3), 930−937.
(42) Cicerone, M. T.; Pikal, M. J.; Qian, K. K. *Adv. Drug Delivery Rev.* **2015**, *93*, 14−24.
(43) Hernandez-Izquierdo, V. M.; Krochta, J. M. *J. Food Sci.* **2008**, *73* (2), R30−9.
(44) Lu, Q.; Hu, X.; Wang, X.; Kluge, J.; Lu, S.; Cebe, P.; Kaplan, D. L. *Acta Biomater.* **2010**, *6* (4), 1380−1387.
(45) Motta, A.; Fambri, L.; Migliaresi, C. *Macromol. Chem. Phys.* **2002**, *203* (10−11), 1658−1665.
(46) Sohn, S.; Strey, H. H.; Gido, S. P. *Biomacromolecules* **2004**, *5* (3), 751−757.
(47) Turhan, K. N.; Sahbaz, F.; Guner, A. *J. Food Sci.* **2001**, *66* (1), 59−62.
(48) Wray, L. S.; Hu, X.; Gallego, J.; Georgakoudi, I.; Omenetto, F. G.; Schmidt, D.; Kaplan, D. L. *J. Biomed. Mater. Res., Part B* **2011**, *99* (1), 89−101.

DOI: 10.1021/acs.biomac.6b01260
Biomacromolecules 2016, 17, 3911−3921